UC San Diego

UC San Diego Electronic Theses and Dissertations

Title
Amphibious Locomotion with a Screw-propelled Snake-like Robot

Permalink
https://escholarship.org/uc/item/19n2n4tv

Author
Lim, Jason

Publication Date
2023

Peer reviewed|Thesis/dissertation

UNIVERSITY OF CALIFORNIA SAN DIEGO

Amphibious Locomotion with a Screw-propelled Snake-like Robot

A thesis submitted in partial satisfaction of the
requirements for the degree
Master of Science

in

Electrical Engineering (Intelligent Systems, Robotics, and Control)

by

Jason Lim

Committee in charge:

Professor Michael Yip, Chair
Professor Nikolay Atanasov
Professor Tania Morimoto

2023

The thesis of Jason Lim is approved, and it is acceptable in quality and form for publication on microfilm and electronically.

University of California San Diego

2023

TABLE OF CONTENTS

LIST OF FIGURES

LIST OF TABLES

ACKNOWLEDGEMENTS

ABSTRACT OF THE THESIS

Amphibious Locomotion with a Screw-propelled Snake-like Robot

by

Jason Lim

Master of Science in Electrical Engineering (Intelligent Systems, Robotics, and Control)

University of California San Diego, 2023

Professor Michael Yip, Chair

Robots that operate in natural environments encounter diverse terrains, ranging from solid ground to granular materials like sand and even full liquids. Various types of robots, including wheeled and legged robots, have been designed to excel in specific domains. Screw-based locomotion is a promising approach for multi-domain mobility, and has been leveraged for amphibious vehicle and robotic designs. Additionally, a snake-like architecture has led to extremely versatile exploratory robots. However, there is limited understanding of the models, parameter effects, and efficiency for multi-terrain Archimedes screw locomotion, and many snake-like robot still face certain limitations.

In this work, we present the design of a mobile test bed, a method to quantitatively

study screw-based locomotion across a wide variety of real-world environments. Our mobile test bed enables indoor and outdoor experimentation, including water tests, to collect data on screw performance. We present experimental results and performance analysis across different media, and analyze the performance of different screw designs to inform optimal design choices. Furthermore, we construct an amphibious screw-propelled snake robot to demonstrate the mobility of screw-based locomotion. The robot is capable of traversing different terrains while maintaining stability and maneuverability. Our experimental results show that screw-based locomotion is effective in multi-domain mobility and can be optimized with specific screw designs. Our findings provide valuable insights into the performance and design of screw-based locomotion for future researchers and engineers. We envision that our results can inform the development of effective screw-based locomotion systems for a range of applications.

Chapter 1

Introduction

One challenge facing mobile robotics is finding a method of locomotion that can efficiently navigate a wide range of terrains. Robots meant for exploration or search & rescue applications need to traverse many kinds of difficult environments, ranging from hard rigid ground, to granular media, to water or viscous liquid. Such robots may also need to climb and navigate obstacles, and fit through tight spaces.

Most mobile robots and autonomous vehicles are designed to operate only in a narrow band of environment types. Active wheels or treads have been well established as an easy, reliable method for traversing hard even ground, and are sometimes used for softer environments such as dirt, sand, and snow [1]. However it can be very difficult for wheeled robots to generate traction in many environments. Treads can provide improved traction, but may have difficulty overcoming obstacles, and neither wheels nor treads are good for swimming. Additionally the only way to overcome more obstacles or softer media is to increase the size of the wheels or treads which can quickly become costly and impractical.

Some bio-inspired locomotion methods have proved successful in navigating more complex terrains. Legged locomotion has shown to be adept at climbing obstacles [2, 3]. In the case of swimming and underwater robots, apart from the obvious designs using standard propellers,

some biomimetic designs have been developed using smart actuators that mimic the efficient locomotion methods of fish and other water animals [4].

Aside from exploratory robots, an area that can benefit greatly from improved robot locomotion is medical robotics. For example, current endoscopes and colonoscopes are limited in their ability to maneuver around tight corners and through convoluted pathways within the body, and most traditional methods of robot locomotion are not suited for such a task. Improved locomotion methods could also be used for autonomous drug delivery or steerable needles.

For exploratory robots, the main limitations of traditional robot designs is that they fail quickly outside the specific environments or media for which they were developed. A great example is NASA's Spirit rover that got stuck in soft sand and had to be decommissioned [5].

ARCSnake is a novel mobile robot design that draws inspiration from two different areas of study that each provide advantages over traditional methods: screw propulsion, and snake-like robots. Archimedean screws as propellers are able to generate propulsion in soft granular media as well as fluid, and modular snake robots have demonstrated success in navigating many different types of difficult environments. By combining screw propulsion with a snake-like backbone, ARCSnake is able to achieve unprecedented versatility and practicality in navigating real world environments, showing great potential for applications like exploration, search and rescue, and disaster relief.. This system also shows the concept for a robotic platform proposal for a NASA mission to search for extant life in the subterranean ocean of Saturn's Moon, Enceladus [6], due to its multi-domain mobility capabilities [7].

While the original ARCSnake design demonstrated promise for a versatile, all-terrain mobile exploratory robot, the full capabilities of screw-based locomotion is still not well understood. Therefore in this thesis we present a method for quantitatively studying screw-based locomotion performance across a wide range of real-world environments in order to better understand the capabilities and limitations of screw-based locomotion. This data will help inform optimal design choices and lead to improved control of ARCSnake and other screw-propelled systems in the

future. Additionally, we detail the design of the amphibious ARCSnake V2 and demonstrate its ability to locomote through sand and water.

1.1 Related Works

1.1.1 Screw Propulsion

Archimedes screws were originally invented for transporting water and continue to be widely used as pumps for all types of fluids and granular media. Over the years, they have also been used as drilling mechanisms, injection molding devices, and turbines [8]. The first applications of screws as propellers were for watercraft [9, 10], and the realization that screws could generate propulsive forces on land led to them being proposed for amphibious vehicles [11]. By the mid-20th century, several screw-propelled vehicles had been developed that demonstrated locomotion and towing capabilities in many types of media, including soil, marshes, snow, and ice [12]. Screw locomotion naturally found its way from large-scale vehicles to smaller mobile robotics [13, 7, 14, 15, 16]. Screw locomotion has also been studied for various medical applications, including endoscopic robots that can navigate the narrow passages and mix of solid and liquid media in the intestines [17, 18, 19], as well as for driving a steerable needle [20]. It is clear that the multi-domain viability of screw propulsion provides many advantages for exploratory mobile robots in situations where traditional methods of locomotion fail. It is still not well understood how screw-locomotion performance metrics, such as generated thrust, degree of slip, and traveling speed, change across different terrains, and how well current models can predict these metrics.

Screws can be thought of as devices that convert rotational force into linear force due to the helical shape of their threads. The physics of screw interaction with a typical threaded nut has been well studied [21]; used in this way, the screw is fully engulfed such that all forces cancel out except in the direction of the screw axis. When screws are used for propelling vehicles or

robots, they often sit on top of or partially submerged in media, and the net force of a single screw cannot be purely along the screw axis. Multiple screws are needed to generate forces in multiple directions, and thus the first screw vehicle designs consisted of two parallel counter-rotating screws [11].

After being empirically shown that screw propulsion is useful for multi-domain mobility, several researchers attempted to model the interaction of screws and deformable media such as sand and water [22, 23]. These first models relied on fairly bold assumptions, for example ignoring the energy imparted to displacement of media and assuming no slip conditions. Other groups have more recently investigated the locomotion characteristics of parallel screw rovers, using simplified kinematic models to simulate locomotion capabilities [24, 15, 16]. In order to forgo some of the assumptions that may lead to an inaccurate model, a model based on terramechanics principles has been proposed in order to capture the relationship of slip and locomotion and account for the energy lost to displacing the media [25]. Screw locomotion models have been experimentally confirmed in a few media such as sand, ice, and water [22, 25, 23]. Additionally, screw locomotion performance has been demonstrated qualitatively but not quantitatively across an even wider variety of terrains [12, 26]. Overall, previous experimental research with screw locomotion has been fairly limited in terms of the metrics used to analyze performance. In order to connect our results with traditional off-road vehicle performance evaluation methods we show a comprehensive set of performance metrics, including novel metrics for screw-based locomotion such as cost of transport.

1.1.2   Snake Robots with Passive Skins

The study of snake-like robots is motivated by the unique abilities of snakes to navigate a variety of complex terrains with minimal structural complexity. Their small cross-sectional profile makes them adept for navigating tight spaces, their bodies can serve as a means for both locomotion and manipulation, and their simple structure is easily scalable [27], opening a wide

range of potential applications including exploration, search and rescue, and medical procedures.

Snakes use various gaits to achieve locomotion in different environments. Serpentine motion, the most common method, is characterized by an s-like curve that is propagated along the body, relying on surface features to push off of and the frictional anisotropy of their skin for propulsion. This wave-like motion is also employed while swimming. Sidewinding is a distinctly different type of motion, in which snakes lift and place sections of their body in parallel tracks to move sideways. This gait is notable for its usefulness in traversing smooth surfaces, granular media, and up inclines such as sand dunes. In tight spaces, snakes may use concertina or rectilinear motion. Concertina motion involves articulating the body into a sinusoidal curve, using the peaks that contact the walls as anchor points while extending the front portion of the body forward. Rectilinear motion, observed only in certain species of large snakes such as boas, is the only gait in which the snake can maintain a straight body posture, moving forward through the active contraction of its ribs and scales, instead of relying on changes in body shape [28].

In an effort to replicate the capabilities of real snakes, modular hyper-redundant snake robots have been developed. An example of biomimicry, most of these robots were designed to mimic the natural gaits of real snakes such as serpentine and side-winding. The performance of these methods of locomotion are heavily dependent on frictional properties, and thus *passive skins* such as wheels and fins are often used to provide the necessary forces for propulsion.

Hirose was one of the first to study the mechanics of snake-like robots, and built several models of ranging capabilities [29]. The first of these models used passive wheels on the bottom of each segment and single axis joints and was capable of simple 2D planar serpentine motion on smooth ground. This design also demonstrated serpentine motion on ice by replacing the wheels with skates [30]. Onal developed a passive wheeled snake robot that utilized soft fluidic elastomer actuators to achieve serpentine motion [31]. Snake robots have also been able to achieve planar serpentine motion by using parallel grooves instead of wheels to maintain frictional anisotropy [32]. Some researchers have explored using surface projections as push-points to propel the robot

forward instead of relying on frictional interaction with the ground [33, 34, 35, 36]. Serpentine motion through a pipe has been demonstrated with a wheel-less snake robot, however this is heavily dependent on the low friction of the surface, and the pipe must still be wide enough to allow the changing body shape [37]. This is a good example of the shortcomings of simple serpentine locomotion: the need for enough room for body shape articulation and the limitation to relatively smooth flat surfaces; performance is significantly affected on even shallow inclines [38].

More versatile snake robots capable of 3D motion have been developed by incorporating extra degrees of freedom in the active joints, through the use of 2-DOF universal joints or 1-DOF joints with alternating axes [29, 39]. This 3D capability is necessary to perform sidewinding motion and can also increase the effectiveness of serpentine motion through sinus-lifting (lifting certain portions of the body to increase the normal force at the contact points) [40]. Wheeled snake robots with 3D capabilities have been shown to successfully climb obstacles, stairs, and traverse uneven surfaces [41, 42]. Additionally wheel-less sidewinding snake robots have been shown to be effective in climbing sandy inclines [43].

It has also been shown that serpentine motion allows snake-like robots swim effectively as well. Kamamichi constructed a purely swimming snake robot using IPCM actuators [44]. Hirose and Ma both developed similar amphibious snake robots that utilize both passive wheels and fins to achieve locomotion on smooth ground and in water [29, 45]. Crespi also developed an amphibious snake robot with passive wheels only that uses a Central Pattern Generator controller to optimize serpentine motion [46, 47].

Snake robots with passive skins are only able to locomote efficiently in a narrow range of environments. These robots must rely on continuously changing their shape, mimicking the gaits of real snakes, in order to generate propulsion, which can be a significant limitation in real world environments. Improvements to the versatility and practicality of snake robots can realized from using active skins.

1.1.3   Snake Robots with Active Skins

Snake robots with passive skins locomote by only actuating the joints between the modules that make up their backbone. Snake robots with *active skins* employ actuators on the exterior of the modules or backbone, and are controlled separately from the joint actuators. This additional level of actuation can lead to improved controllability and allow snake robots to navigate more difficult and complex terrains. The key feature of active skin snake robots is that they no longer rely on articulating their body into a specific shape or gait pattern to locomote; instead the active skin propels the robot forward while the joints can be used to steer and conform the body shape to its environment.

The simplest implementation of active skins are active wheels instead of passive ones. Hirose developed the ACM-R4.1, which featured active wheels oriented in both the yaw and pitch axis to allow very versatile motion, such as navigating a narrow straight pipe with sharp turns [29]. The thin wheels however got too easily stuck on projections in rough terrain and slipped on sand and grass, leading to the design of the ACM-R4.2. This version removed the yaw axis wheels to allow room for larger wheels with better traction, and demonstrated success in traversing gaps, rough terrain, and climbing over obstacles [48]. The GMD-SNAKE2 featured an array of small active wheels that completely surrounded each segment, allowing the wheels to provide propulsion no matter which side of the robot contacted the environment [49]. Implementing active wheels is a significant step towards expanding the range of locomotive capabilities, but these robots are still restricted to firm, dry environments in which the wheels can gain traction and not get stuck.

Another method that even further improves a robot's ability to traverse difficult terrain is the use of active treads. Hirose developed several iterations of the Souryu robot that featured active treads circulating length-wise on the dorsal/ventral sides of each segment, with 2-DOF joints connecting each segment for steering and body articulation [29, 50, 51]. Borenstein developed the OmniTread snake robot with active treads and pneumatic bellow joints, for which the key

innovation was the implementation of active treads on all four sides of each segment, which allows for propulsion no matter the orientation of the robot along the roll axis, as the robot often rolls over on rough obstacle-ridden terrains [52, 53]. These robots have shown impressive success in traversing difficult environments, such as natural rocky, sandy, and brush terrain, stair climbing, navigating through raised holes, and climbing steeper inclines and even vertical pipes.

Other interesting implementations of active skins include an active screw drive mechanism composed of passive wheels [54], a rope drive system [55], and a toroidal skin drive mechanism that envelops the entire length of the robot [56]. The latter two designs are notable for being much more compact that active wheels or treads, allowing motion through dense underbrush in which wheels and treads may get stuck.

These active skin robots solve some of the important shortcomings of snakes with passive skins. They allow locomotion through narrow passages and improve performance over rougher complex terrains and obstacles, although certain environmental limitations still persist. Active wheels and treads may have difficulty in environments that provide little to no traction such as very loose sand and snow, and have an issue of debris clogging the drive systems. Additionally many of these robots are still designed for land use only and fail outright in fluidic environments. In the next section we introduce our proposal for an amphibious snake robot with a novel active skin that allows for locomotion in an unprecedentedly wide range of environments.

1.2   ARCSnake V1

The recently developed ARCSnake combines a snake-like backbone with a novel active skin using Archimedean screws. This allows for an extremely versatile robot that can locomote through a wider range of environments than existing mobile robots. Previously a first iteration, ARCSnake V1 [7, 13], has been designed and constructed, consisting of 4 segments connected by universal 2-DOF active joints (U-joints). An Archimedean screw shell envelops each segment

Figure 1.1: ARCSnake V1 showcases the multi-domain ability of a screw-propelled snake robot, which can even grip and climb a pole (right).

providing propulsion. The inner core of each segment houses the electronics and motors that power both the U-joint motors and screw shell motor.

ARCSnake V1 has demonstrated successful locomotion in a variety of media such as sand, gravel, grass, dirt, and concrete. By changing its configuration it is able to perform many different modes of locomotion. For example on hard concrete, where the screws can not gain traction, it can configure into an M-shape and utilize the screws as wheels instead. It can also perform side-winding, move through narrow passages, grip and climb large pipes, and climb stairs. Using screws that continuously surround the segments allow for propulsion regardless of orientation. Additionally the screws can act as propellers in fluidic environments, allowing for amphibious locomotion with future waterproofed versions. The experiments detailed in this thesis help expand on the work for ARCSnake through quantitative analysis of screw-based locomotion. These results give a better understanding of the capabilities and limitations a screw-propelled robot like ARCSnake would face in different environments.

Portions of Chapter 1 are a reprint of material as it appears in the following paper pending publication: Jason Lim, Calvin Joyce, Elizabeth Peiros, Mingwei Yeoh, Peter V. Gavrilov, Sara G. Wickenhiser, Dimitri A. Schreiber, Florian Richter, Michael C. Yip. "Mobility Analysis of Screw-Based Locomotion and Propulsion in Various Media", IEEE International Conference on Robotics and Automation, 2023. The thesis author was the principal author of this paper.

Chapter 2

Testbed Experiments

In order to investigate the behavior of screw locomotion in various media a mobile test bed is constructed. The mobile test bed is intended to characterize the performance of screw locomotion by collecting force and velocity data from a test screw rigidly attached to the test bed. Experiments are carried out in a variety of dry environments as well as water. There are several goals for these experiments:

1. Investigate how the locomotion performance responds to varying input controls.

2. Compare the baseline performance across different environments.

3. Compare results from various screw geometries to inform optimal screw design choices, which may vary depending on the environment.

2.1   Mechanical Design

An overview of the test bed design is shown in Fig. 2.2. To ensure high quality measurements across a large range of media, the test bed must have the following requirements:

- Constrain the motion to a single, linear axis to isolate the locomotion measurement.

- Light weight and easy to reposition for both indoor and outdoor experiments.

- Apply axial loads to simulate towing.

- Sufficient stiffness such that deflection does not impact experimental data.

- Measure the screw's velocity and applied torque.

- Measure the resulting screw-locomotion's velocity and applied forces and torque.

To constrain the locomotion to a single, linear axis and keep the structure light weight, a linear rail Ball Bearing Carriage for 23 mm Wide Rail 6709K16 with 1600 mm length is mounted on "T-Slotted Framing Double Six Slot Rail, Silver, 3" High x 1-1/2" Wide, Hollow" (47065T108). Similarly, the legs of the test bed are made with "T-Slotted Framing Silver Diagonal Brace for 1" High Single Rail, 12" Long" (47065T188). To measure traveling velocity, an additional motor, RMD-L 7015, is mounted to the carriage of the horizontal linear rail and can be held passive or regulate a torque to apply an axial load on the system. The RMD-L 7015 is selected due to its high transparency since it is brush-less and does not have an internal gearbox. Another vertical linear rail, 23 mm Wide Guide Rail for Ball Bearing Carriage 6709K53, is attached to a Ball Bearing Carriage with Flange for 23 mm Wide Rail 6709K15, which is mounted to the horizontal rail's carriage. The vertical linear rail allows for freedom of motion in the vertical axis to compensate for uneven surfaces being experimented on. Additionally, this degree of freedom allows the effective mass of the screw to be varied which may be an important factor in performance. Different screw drive configurations can be attached to the end of the vertical rail for different experiment modes. Three different screw drive configurations will be used: a single screw configuration for land experiments, a double screw configuration, and a belt drive configuration for water experiments.

All the mechanical design choices are validated for minimal deflection with a Finite Element Analysis (FEA) as shown in Fig. 2.1. The maximum deflection from the FEA is less than 0.3 mm which is sufficiently low for locomotion experiments.

URES (mm)

2.237e-01
2.013e-01
1.789e-01
1.566e-01
1.342e-01
1.118e-01
8.947e-02
6.710e-02
4.474e-02
2.237e-02
1.000e-30
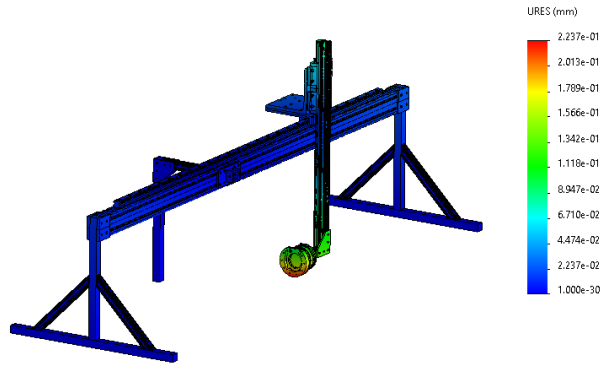
Figure 2.1: FEA on mobile test bed where the 5 Nm is applied on where the screw would be located. The direction and magnitude of the applied force in this analysis is a worst case scenario and sufficiently larger than what will be seen in the experiments.

2.1.1   Sensors

The screws are driven with the RMDx8 Pro motor which provides velocity measurements from a quadrature optical encoder to measure the screw's angular velocity. The RMD-L 7015 motor attached to the horizontal rail carriage is used to measure the linear traveling velocity and applied drawbar force. Finally, a 6-DoF Force Torque Sensor (FTS), the Axia80 (ATI Industrial Automation), is used to measure the screw's applied torque and the resulting screw-locomotion forces.

2.2   Single Screw Land Experiments

As shown in Fig. 2.2 the single screw configuration for the land experiments consists of mounting the screw shell directly to the motor, which is connected to the sensor and then the vertical rail via a small segment of the same rail part. This configuration is meant to measure the forces and torques produced by a single screw propeller during locomotion as well as a static case on land environments.
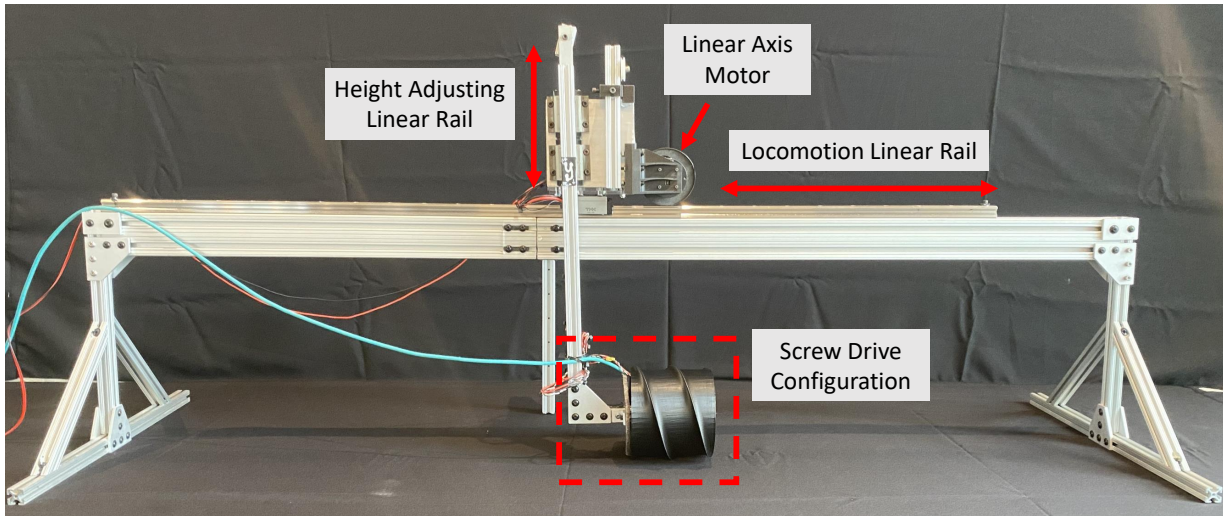
Figure 2.2: The mobile test bed is designed to carry out experiments on a myriad of indoor and outdoor environments. Different screw configurations can be attached to the vertical rail to handle land and water, and explore different modes of screw locomotion like a parallel double screw, which is a common configuration found in existing screw-based robots.
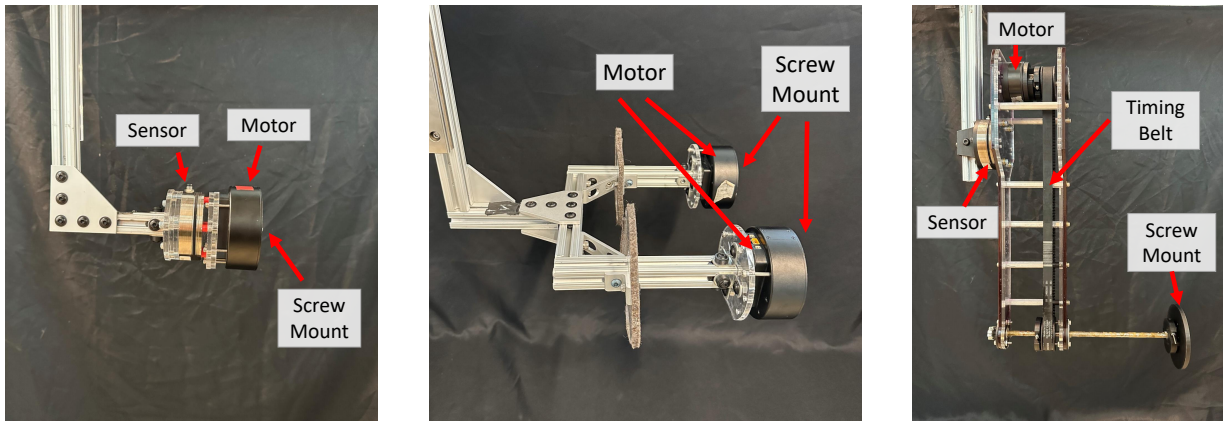
Figure 2.3: Three different screw drive configurations are attached to the test bed: Single Screw (left), Double Screw (middle), and a Belt Drive configuration for water experiments (right).

2.2.1 Performance Evaluation Metrics

The screw performance is evaluated in static and motion scenarios. The test bed supports both of these metrics by simply locking/unlocking the locomotion linear rail. The metrics are inspired from both screw and conventional vehicle locomotion analysis hence providing good coverage of metrics to understand screw-locomotion across different media.

Static Performance

For typical screws in a threaded environment, the relationship between input torque and the amount of force generated in the axial direction can be described by the mechanical advantage (MA). Derived from conservation of energy principles, mechanical advantage is:

$$MA = \frac{F_{thrust}}{\tau_{in}} = \eta_s \frac{2\pi}{\ell},$$

(2.1)

where F_{thrust} is the thrust force measured by the FTS, τ_{in} is the torque applied by the screw motor, η_s is the static efficiency, and ℓ is the longitudinal distance a thread spans in one full revolution around the screw (i.e. pitch times number of thread starts). Mechanical advantage is heavily dependent upon the frictional properties of the media. For media that is not perfectly rigid, additional efficiency losses may result from deformations of the media, and therefore η_s can be treated as term that encompasses any type of energy loss to surroundings. Comparing the mechanical advantage and efficiency of the screw across different media provides insight into the performance of the screw in a static scenario.

Motion Performance

The ideal locomotion velocity is given by assuming that the screw threads move through grooves as if it were in a threaded nut. Therefore, the ideal velocity for a screw can be computed

geometrically as follows:

$$v_{ideal} = \frac{\omega \ell}{2\pi} \tag{2.2}$$

where ω is the angular velocity of the screw motor. From the ideal velocity, a longitudinal slippage can be defined as:

$$s = \frac{v_{ideal} - v}{v_{ideal}}, \tag{2.3}$$

where v is the measured velocity from the screw-locomotion. The slip factor equals 1 when the screw slips uncontrollably and doesn't move at all, and equals 0 when the screw moves at the ideal optimal velocity hence giving a good metric about motion capabilities of screws in different media.

From the measured traveling velocity, the locomotive efficiency of the system, η_m, is calculated as

$$\eta_m = \frac{F_{thrust} v}{\tau_{in} \omega} \tag{2.4}$$

and the cost of transport, COT, is calculated as

$$COT = \frac{P_{in}}{mgv}, \tag{2.5}$$

where P_{in} is the power input to the system, m is mass (i.e. screw(s) and motors), and $g = 9.81 \ m/s^2$. Locomotion efficiency is different from static efficiency, η_s, since it incorporates motion. Cost of transport is a dimensionless quantity related to energy efficiency that allows for comparison among different modes of locomotion.

2.2.2 Experimental Setup

To ensure consistent results, the following experimental setup steps are taken after placing the mobile test bed:

1. Flatten and level the media to achieve as uniform conditions as possible.
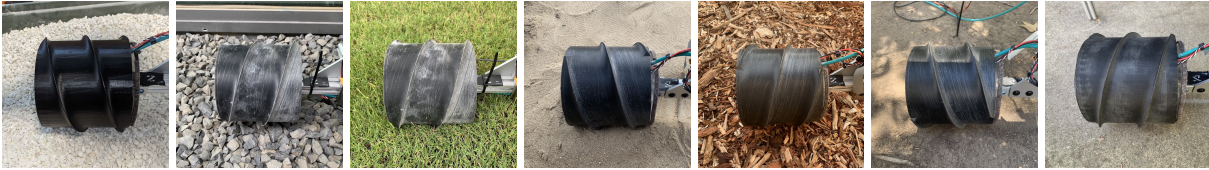
Figure 2.4: Representative images of the test bed experiments conducted in the following media (from left to right): small gravel, big gravel, grass, sand, wood chips, dirt, and concrete.

2. The height adjustable linear rail is locked such that the screw(s) are free hanging. A "free hanging" measurement from the FTS is taken to capture any potential drifts between trials.

3. The height adjustable linear rail is unlocked and the screw is set down on the media. A "set down" measurement from the FTS is taken to measure any pre-loading from the media on the screw.

4. The FTS sensor is zeroed to then measure differential measurements.

From this point, the screw motor can be driven to begin the experiment.

2.2.3 Results of Single Screw Experiments

Fig. 2.4 depicts the many types of land environments on which the screw is tested. These experiments characterize the locomotion performance by measuring the velocity and output forces of the screw in these different media. We also experiment with a parallel screw configuration to show how the single screw measurements can be used to estimate performance of previously developed screw-based locomotion systems [11, 24].

We estimate the coefficient of friction on each media by replacing the screw with a smooth cylinder of the same material. Driving the screw motor at a constant velocity, the coefficient of friction, μ_f, can then be estimated as

$$\mu_f = \frac{\tau_s}{mgr},\tag{2.6}$$

where τ_s is the torque about the screw axis measured by the FTS, and r is the radius from screw

Table 2.1: Results from linear motion experiments with and without an axial load applied.

Media	Coefficient of Friction	Longitudinal Slippage		Thrust in Motion		Locomotive Efficiency		COT	
		No Load	*w/ Load*	*No Load*	*w/ Load*	*No Load*	*w/ Load*	*No Load*	*w/ Load*
Small Gravel	0.32 ± 0.01	0.37 ± 0.10	0.42 ± 0.12	5.63 ± 0.9	16.9 ± 1.2	0.059	0.17	2.44	2.53
Big Gravel	0.23 ± 0.03	0.36 ± 0.18	0.49 ± 0.24	6.99 ± 1.9	18.0 ± 2.8	0.093	0.17	1.91	2.79
Grass	0.38 ± 0.05	0.52 ± 0.17	0.48 ± 0.19	7.32 ± 1.2	18.5 ± 1.8	0.046	0.17	4.03	2.84
Sand	0.48 ± 0.03	0.30 ± 0.04	0.63 ± 0.27	8.53 ± 1.0	9.67 ± 1.6	0.082	0.05	2.63	5.24
Wood Chips	0.31 ± 0.04	0.34 ± 0.12	0.46 ± 0.24	7.21 ± 1.5	18.1 ± 2.8	0.092	0.20	1.99	2.30
Dirt	0.38 ± 0.02	0.36 ± 0.16	0.47 ± 0.24	9.06 ± 1.8	11.4 ± 2.2	0.092	0.099	2.50	3.08
Concrete	0.34 ± 0.03	0.99 ± 0.02	NA	2.15 ± 0.5	NA	0.0003	NA	NA	NA

axis to the contact point.

The screw used for these experiments is 3-D printed ABS with a root radius 77.5 mm, outer radius 86 mm, lead angle 16°, total length of 147 mm, and two thread starts. These screw parameters are selected since they have been shown to be most efficient in generating thrust force [21] and have been the standard parameters for recent screw-based systems [8, 13]. Further explanation of screw geometry is given in the appendix. In order to process the raw data from the test bed for analysis, the data from the motors and FTS are passed through a low pass filter with a cutoff frequency of 6 Hz and sampling frequency of 125 Hz. The data is clipped manually to only include the steady state portion of the experiment.

Single Segment Static Tests

For this experiment, the goal is to measure the maximum thrust produced for a given input torque under static conditions. All degrees of freedom are restricted except for the vertical direction so that the screw is still allowed to sink into the media. Torque is applied such that screw may spin initially but eventually gets stuck and a steady state, static condition exists. Therefore, the screw motor's max torque for this experiment is set such that the screw remains static in the media being tested on. The ratio of thrust measured during this steady state and the input torque is the MA of the screw, and varies depending on the properties of the media. Results are shown in Fig. 2.6.

Figure 2.5: During the load experiments, in sand (left) the screw quickly dug itself deeply into the material, and in dirt (right), the screw dug itself into a rock bed, both of which caused slippage on the linear axis motor leading into inconsistent velocity readings. Therefore a lower axial load of 6N instead of 12N was used for these media.

Single Segment Motion Tests

This experiment allows freedom of motion in both the axial and vertical directions, so that the speed of travel can be measured and sinkage into the media is still allowed, while all other degrees of freedom are restricted by the test bed. The screw motor is set to regulate at a constant velocity: 2, 3, 4, 5, and 6 rad/s. The measured locomotion velocity, motor torque, angular velocity, and force measurements allow the calculation of metrics such as longitudinal slip, net thrust (also called drawbar pull), locomotive efficiency, and cost of transport. Furthermore, we repeat the experiments with and without an axial load. The axial load is set to 12N except for the sand and dirt tests where a load of 6N is used. A lower axial load is required for sand and dirt because at 12N, the screw would dig itself in as shown in Fig. 2.5, leading to inconsistent results. The results are shown in Fig. 2.7 and Table 2.1. Note that the concrete results are incomplete due to the lack of mobility the screw provided on that media.
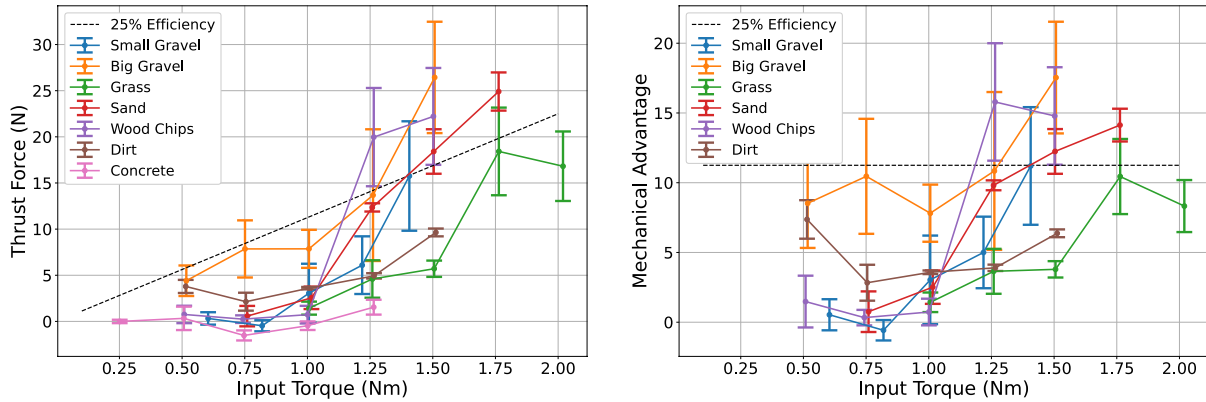
Figure 2.6: The left and right plots show the Thrust Force and MA, respectively, for different input torques in a static condition. The max torque tested on is the maximum torque the screw is held static for the media.
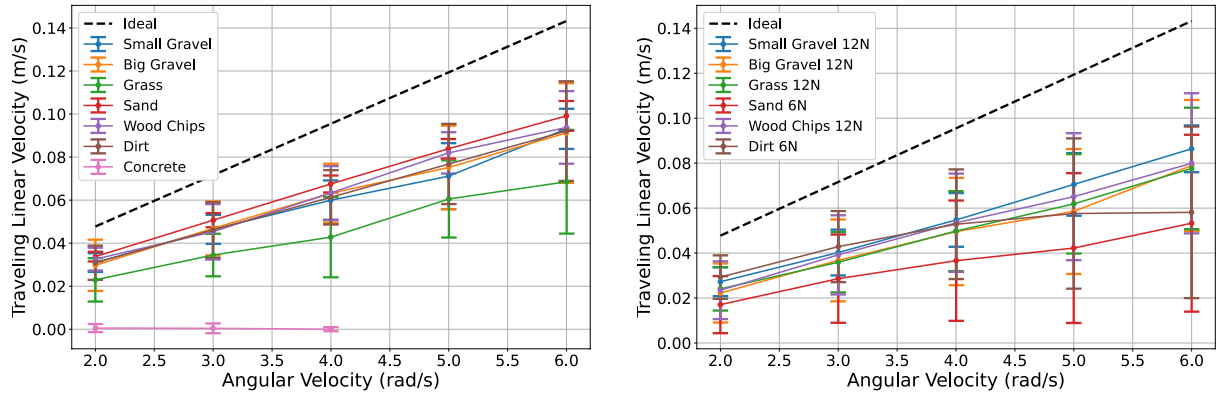
Figure 2.7: The left and right plots show the linear traveling velocity as a function of input angular velocity with and without an axial load, respectively. As visible from these plots, the linearity of the velocity relationship holds true across all media except concrete which never produced any motion.

2.2.4   Double Screw Experiments

A parallel screw configuration is attached to the test-bed as shown in Fig. 2.8. With this modification, the FTS has to be removed; hence we only collect measurements from the screw and linear axis motors. The media used for these experiments is small gravel and small gravel & sand. The screws are set to regulate a constant velocity of: 2, 3, 4, and 5 rad/s. The measured locomotion velocity is shown in Fig. 2.9, compared with the results of a single screw. The measured longitudinal slippage and COT are 0.33 ± 0.07 and 2.45, respectively, for the gravel

Figure 2.8: Figures from the parallel configuration experiments where the media is small gravel and small gravel & sand as shown in the left and right figures, respectively.

and 0.29 ± 0.04 and 2.28, respectively, for the gravel & sand.
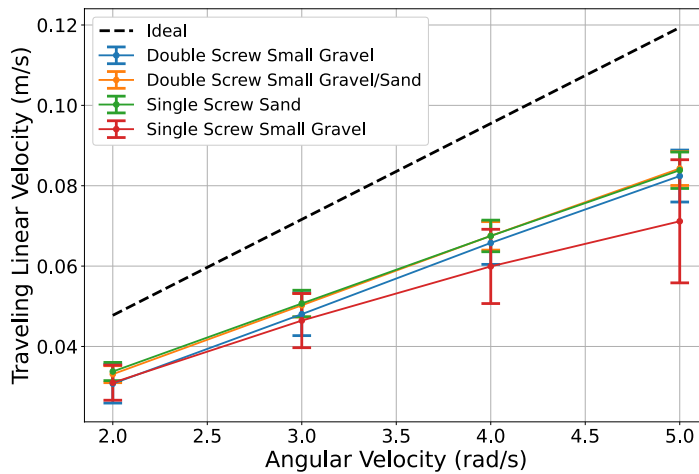

Figure 2.9: The plots show traveling velocity and longitudinal slip as a function of input angular velocity from our parallel configuration experiment. We also include the single segment results in the corresponding media to provide perspective about how our experimental results correlate with screw-based locomotion systems.
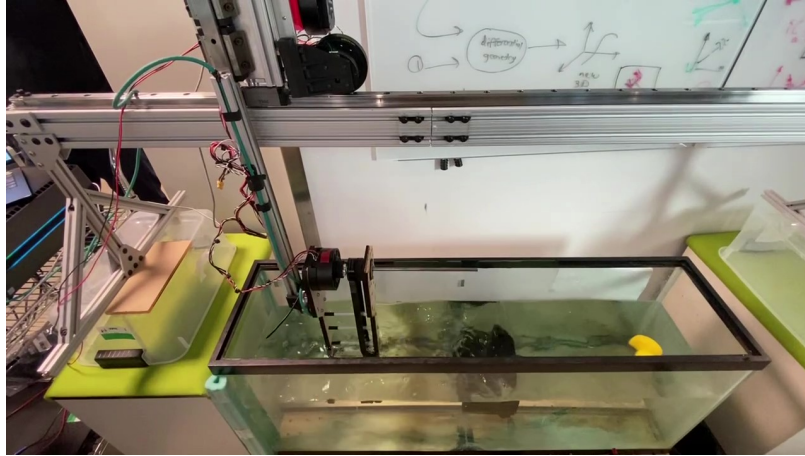
Figure 2.10: Setup of the water experiments with the water tank and belt drive configuration.

2.3   Water Experiments

Previous work has shown that the blade height and lead angle of the screw threads are the most influential parameters in determining locomotion performance [22, 14, 57]. The screws used for ARCSnake V1, which was not designed for water use, and the land experiments had very small blade height of 8mm. We hypothesize that ARCSnake V2, which is planned for amphibious locomotion, will need bigger blades in order to produce significant thrust in water, however it is unclear what lead angle should be used. Thus these water experiments are performed with three different screw shell designs with a larger blade height of 30mm and lead angle of $7°$, $15°$, and $30°$, to analyze the effect of lead angle on water performance, and they are compared to the original screw design used for land experiments. In order to protect the sensor and motor from water damage, a timing belt is used to drive the screw underwater for these tests. Fig. 2.3 shows the mechanical design of the configuration. The RMD L-7015 motor is connected via 3D printed belt pulleys to a High-Strength Timing Belt (1000-5M-15) that drives a shaft to which the screw shells can be mounted. The setup is held together by two acrylic plates that is designed to have as little drag effect as possible. Experiments are performed in a $13 \times 48 \times 21$ inch water tank. The setup of the experiment is depicted in Fig. 2.10.
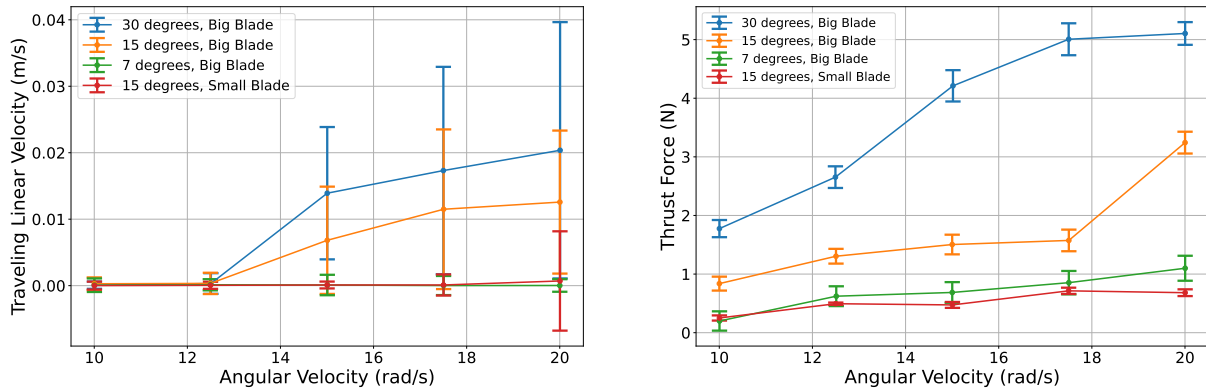
Figure 2.11: The left and right plots show the linear traveling velocity and thrust force, respectively, as a function of input angular velocity for different screw designs in water, where the angle refers to lead angle. Big blade refers to a blade height of 17.5mm, and small blade refers to a blade height of 5mm.

2.3.1   Experimental Procedure for Water Tests

The experimental procedure for water tests is simple as there is no pre-loading effect on the screw. The belt drive configuration is lowered into the water tank so that the screw is fully submerged, the sensor is biased, and then the motor is regulated at a constant angular velocity. When measuring thrust force, the horizontal linear rail is locked to restrict motion in order to measure the maximum thrust that the screw can produce.

2.3.2   Results for Water Tests

Fig. 2.11 shows the results of the water experiments. From these plots it is clear that a larger lead angle leads to significantly increased performance, achieving much higher thrust forces per input angular velocity. This makes sense, as a steeper angle of the threads will force fluid along the axis at a faster rate given a particular angular velocity and thus produce more force due to conservation of momentum. For the screws with the 7° lead angle and big blade, and 15° lead angle and small blade, the force that they produced was not enough to overcome the frictional resistance between the carriage and linear rail, and thus show approximately zero traveling velocity, although it is clear from the thrust force plot that they still produce some

22

amount of thrust force. It is important to note that for the application of driving a robot in water, as long as an external load is not applied, the resistance will be much less than that of the carriage/linear rail, and therefore these screw designs may still be a viable option.

2.4 Discussion

The static test results highlight two essential properties: a max applied and resultant torque exists when remaining static in different media, and the MA increases with the input torque when remaining static. This implies that maximal static efficiency is achieved at the transition point directly below the maximum environment-dependent torque. From the screw velocity plots in Fig. 2.7, it is apparent that the input-to-output velocity relationship is linear even with an axial load. The axial load, however, does increase the longitudinal slippage, thrust in motion, locomotion efficiency, and COT, as seen in Table 2.1. The increased thrust in motion is due to the screw working to overcome the axial load. However, producing this extra thrust does not require much additional input torque from the motor; thus, the efficiency also increases. This may be partially explained by the axial load causing the screw to embed better into the media, gaining more traction and generating better propulsion. There is a limit to this effect, however, as if the screw digs itself in too much, then overall performance drops significantly, as shown in the sand test.

As expected, screws cannot provide any locomotion on rigid surfaces such as concrete. Meanwhile, the more granular media such as gravel and wood chips have the highest locomotion efficiency when under axial load and the lowest COT. We believe this occurs because these media have a higher shearing force and provide better traction. Sand, on the other hand has a significant drop in locomotive efficiency when an axial load is applied, and we believe this is because the screw digs itself too much into the media, as seen in Fig. 2.5. These are crucial phenomena for future screw-based locomotion systems to understand as it implies a limit to the amount of towing

ability (axial load) in highly granular environments like sand. Another result of note is not just the average longitudinal slip; the standard deviation indicates how consistently the screw can locomote well. Locomotion on media with a high standard deviation of longitudinal slip, such as gravel, indicates that the screw's velocity is erratic. While the gravel's high shearing force and low friction provided a good performance overall, the erratic motion behavior may be undesirable under specific scenarios.

The parallel configuration experiments highlight how our results correspond to previously proposed screw-locomotion systems [11, 24]. The results line up with the single segment experiments; however, a slight performance increase is seen in longitudinal slip and increased COT, likely due to the averaging effect of counter-rotating parallel screws.

The two most influential media properties affecting performance are frictional resistance and shearing strength. High frictional resistance reduces efficiency and mechanical advantage, while a low shearing strength allows the screw to displace media more easily, also leading to reduced efficiency. Another critical factor that is not explored here is the effect of the weight of the screw configuration. Preliminary tests showed that decreasing the vertical normal force significantly reduced the thrust produced and increased the longitudinal slip.

The main finding of the water experiments was that lead angle is an extremely influential design parameter for performance in fluids. Confirming the findings of previous research [22, 57], a larger lead angle leads to a higher thrust force. It is also clear that a bigger blade height leads to better performance, however it should be noted that a big blade height may not be able to compensate for lead angle that is too small, as seen by the closeness of performance in the $7°$, big blade screw and $15°$, small blade screw. These results suggest that it is possible to achieve a decent amount of thrust with very small blades if the lead angle is high enough.

While one of the goals of these experiments was to also compare the performance of different screw designs across all of these environments as well, at the time of writing this thesis these experiments have not yet been completed. The screw designs with larger blade height and

lead angles produced so much force that the mobile test bed broke and needed to be repaired. However, while this precluded us from collecting accurate force and velocity data, we were still able to qualitatively observe the performance of a screw with bigger blades in sand, and found that if the blades are too big that the screw will excavate an excessive amount of sand and is unable to locomote forward. This is important because it suggests that there is a trade-off between optimal design parameters for water and sand. In water the best performance is clearly achieved with a large lead angle and large blade height. However, preliminary tests suggest that a large lead angle and large blade height may cause the screw to dig itself into sand too quickly and severely inhibit the locomotive capabilities. More experimentation must be done to find the optimal balance for these parameters if the screw needs to operate well in both sand and water.

Portions of Chapter 2 are a reprint of material as it appears in the following paper pending publication: Jason Lim, Calvin Joyce, Elizabeth Peiros, Mingwei Yeoh, Peter V. Gavrilov, Sara G. Wickenhiser, Dimitri A. Schreiber, Florian Richter, Michael C. Yip. "Mobility Analysis of Screw-Based Locomotion and Propulsion in Various Media", IEEE International Conference on Robotics and Automation, 2023. The thesis author was the principal author of this paper.

Chapter 3

ARCSnake V2

The second main contribution of this work is the assembly and testing of ARCSnake V2, the second iteration of our snake-like screw-propelled robotic system that is waterproofed and designed for amphibious and all-terrain locomotion. This section will detail the mechanical design and assembly, including the steps taken to validate the waterproof seals, and discuss the results of preliminary testing with the robot in water.

3.1   Mechanical Design

Fig. 3.1 shows an overview of the segment design for ARCSnake V2. The motor that drives the screw shell and all electronics are mounted to a 3D-printed "screw block" (printed with Grey Pro resin on a Formlabs printer), which is slotted into a polycarbonate inner tube housing and sealed with a rubber gasket. Two joint-to-body mating parts (printed with Grey Pro resin on a Formlabs printer) are adhered with high-strength epoxy to the ends of the tube housing, to which the half universal joints (U-joints) are mounted and sealed with an O-ring. Two High Precision Crossed Roller Bearings (JA060XP0) are mounted on the ends of the tube housing, onto which fit the outer screw shell, which is printed in four pieces with PLA. The outer screw shell has a lead angle of 15°, blade height of 50mm, and two starts. These parameters were picked to be a

balance between the optimal choices for sand and water as discussed in the previous section.

Fig. 3.2 shows the design of the screw block and half joint in detail. The interior of the screw block contains an Gyems RMD L-7015 brushless motor that drives the external sun gear shaft via timing belt (90XL037). The shaft is sealed with a Spring-Loaded Rotary Shaft Seal (5154T47), and Permatex 80022 Blue RTV Silicone Gasket Maker is used to seal the edges between the shaft seal and screw block. The exterior of the screw block contains the external sun gear, Blue Robotics cables and penetrators, and a push-to-connect fitting for a positive pressure pneumatic line. The half U-joint contains a Gyems RMD X8-Pro Actuator mounted to an aluminum joint frame. The joint motor drives a pulley system that uses a Dyneema DM20 cable and pulleys for and additional gear reduction in addition to the actuator's internal gearbox.

Fig. 3.3 shows a complete segment without the screw shells. The half U-joints are connected orthogonally to complete the robot with three segments, shown in Fig. 3.4. The power and communication cable connections between segments are sealed using Moisture-Seal Heat-Shrink Tubing.

3.2   Field Tests

After completing the assembly ARCSnake V2 was taken to be tested on a sandy beach, shown in Fig. 3.5. Unfortunately we ran into motor issues, where the motors would shut off when the current would spike too high. We believe this was due to increased electrical resistance in the long tether cables, leading to a voltage drop at the motors which raised low-voltage errors in the motor's firmware. Therefore we were only able to spin two out of the three screws at a reasonable speed which limited the robot's ability to locomote over the compact sand, although we still demonstrated that two screw segments could provide enough propulsion to locomote in water. We also showed the joints could be actuated to demonstrate snake-like capability through undulation of the U-joints.
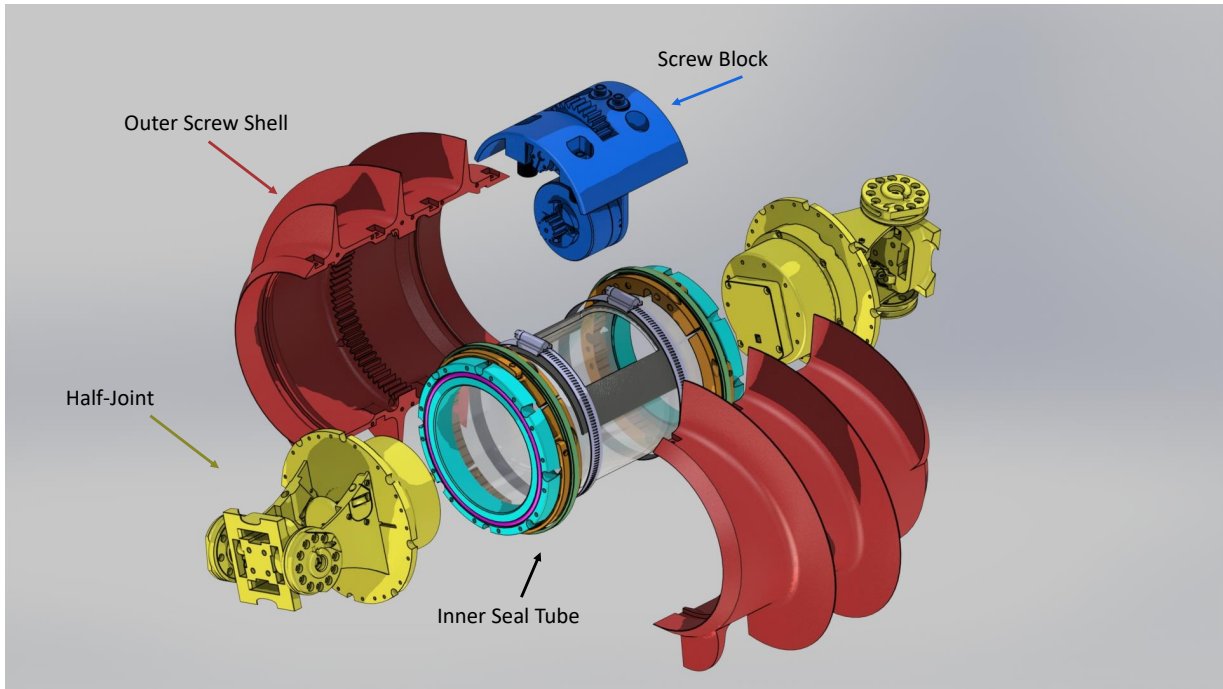
Figure 3.1: An exploded view of the CAD model for a segment of ARCSnake V2.
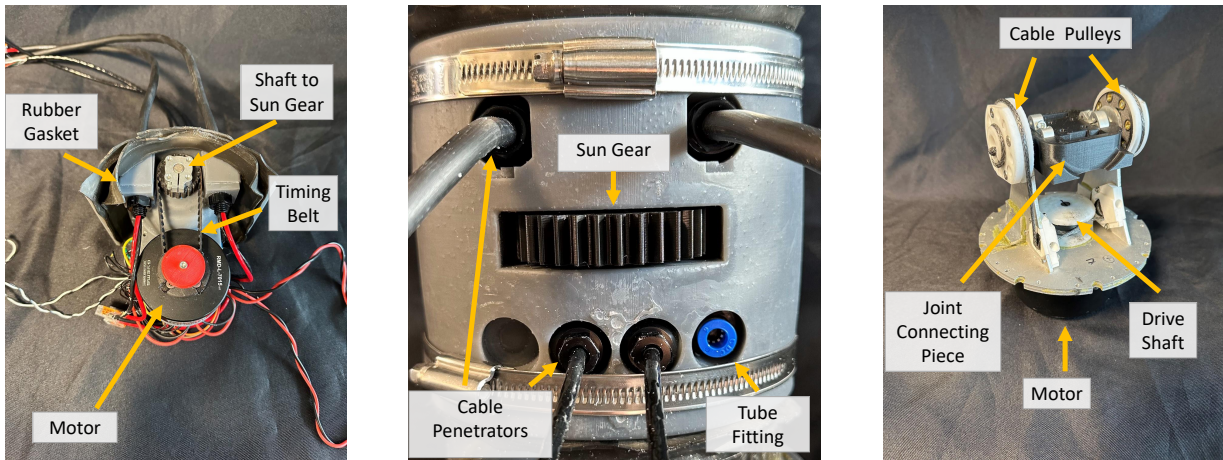
Figure 3.2: The screw block contains the motor that drives the screw shell and all of the electronics on the interior (left), and the sun gear that couples to the screw shell, cable penetrators, and a tube fitting for the positive pressure line on the exterior face of the screw block (middle). The half U-joint (right) consists of the joint motor, cable drive, and connecting piece.
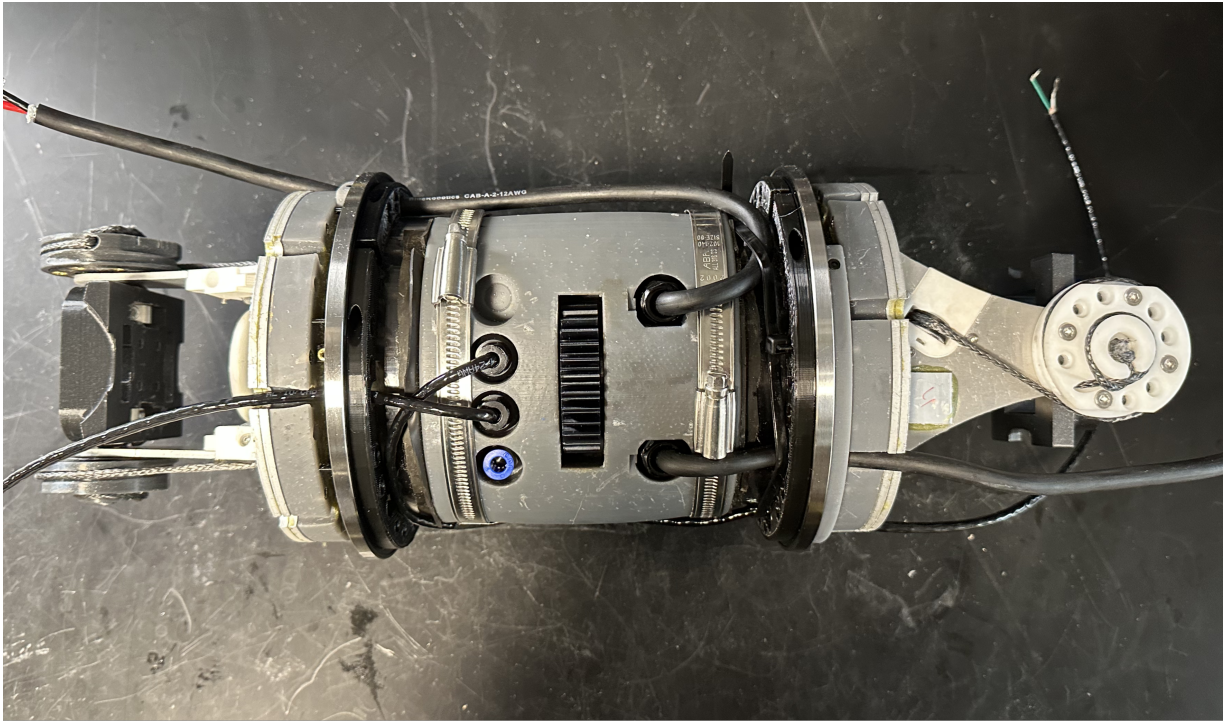
Figure 3.3: A fully assembled segment of ARCSnake V2.
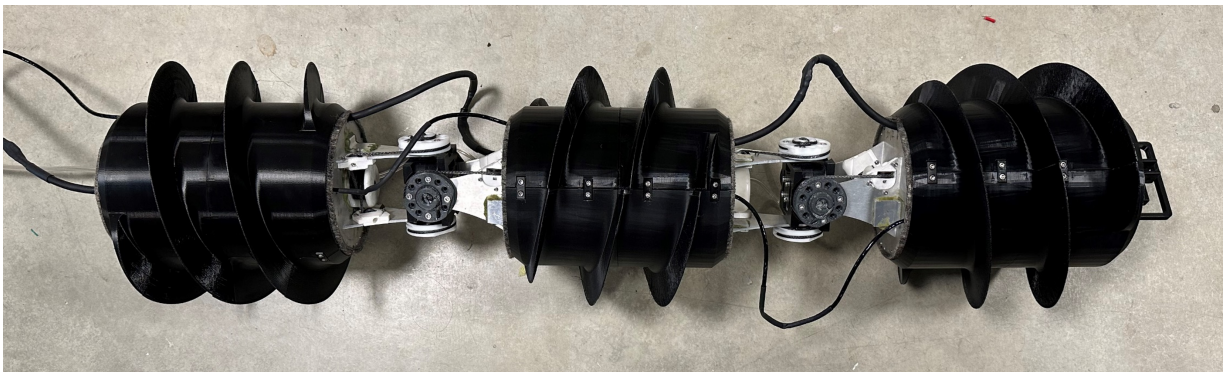
Figure 3.4: The fully assembled ARCSnake V2 with three segments.

Figure 3.5: Testing ARCSnake V2 at Mission Bay, San Diego. The robot is tethered to a desktop computer, power supply, and air compressor (right).

Figure 3.6: ARCSnake V2 demonstrated swimming capability even with only two screws spinning (left). However, due to motor issues the screw shells could not be driven strong enough to screw through the wet compact sand (right).

Chapter 4

Conclusion

In conclusion, this thesis expands upon the research into developing a novel multi-domain mobile robot that combines screw propulsion with a hyper-redundant snake-like architecture. It has been previously demonstrated that screw-propulsion can be used for amphibious locomotion in granular media and fluids. However, the field lacks comprehensive quantitative studies into the performance of screw-based locomotion, which is important for understanding the limitations and capabilities of screw-propelled robots in different environments. Attempting to fill this gap, one of the main contributions of this thesis details the design of a mobile test bed: a method to scientifically and quantitatively study the performance of screw locomotion across a wide range of real-world environments, including land terrains as well as fluid. Preliminary experiments are carried out that demonstrate the utility of the mobile test bed, and the results lead to some initial insights of what media properties and screw design parameters are most influential for screw locomotion performance. The second main contribution of this thesis is the design and construction of ARCSnake V2, the second iteration of a screw-propelled, snake-like robot. This robot was designed to be able to locomote through a vast range of environments, including many kinds of land environments such as hard smooth ground and granular media such as sand and snow, as well as water/fluids. Its snake-like architecture enables it to navigate obstacles

and provides versatility and capability for navigating and climbing obstacles, while the screw-propelled segments allow for propulsion in granular media and fluidic environments. The robot can reconfigure itself for different modes of locomotion, which adds to its versatility. This robot is envisioned to solve some of the limitations of traditional mobile robots, and could potentially be very useful in applications such as search & rescue, disaster relief, sea and cave exploration, and space exploration.

4.1 Key Findings on Screw Locomotoin

One of the key insights gained from these test bed experiments is what media properties most influential for locomotion performance. The results suggest that the highest locomotive efficiency, defined as the ratio of output power of the screw to the input power to the motor, is achieved on media that have low coefficients of friction and a high shearing force, such as gravel and compact dirt. A low coefficient of friction is important as the screw threads must slide through the media as the screw rotates, in contrast to typical wheeled locomotion in which higher friction leads to better traction. Thus it is also important that the media have a high shearing force as to provide significant reactionary force as the screw threads shear through the media. If the shear force is not high, such as the case in loose sand, the screw will lose energy to the displacement of the media and end up digging itself into the media. This may be aided by the use of bigger blades, and in our future work we would like to explore the effect of "digging in" in depth.

In terms of screw design parameters, it is clear that of the parameters tested the best performance in water was the largest lead angle ($30°$) and large blades. This does seem to be on the opposite spectrum as sand. While we were unable to obtain definitive quantitative evidence at the time of writing this thesis, from a few qualitative tests it seemed that larger lead angle and blade height led to decreased mobility in sand, as the screw would excavate a lot of sand very quickly. Further experimentation should be done in order to determine an optimal balance

between sand and water performance for an amphibious screw-propelled robot. Additionally, we observed that an influential parameter not mentioned in previous literature may be the spacing between screw blades, which is dependent upon the lead angle and number of starts. Small spacing between the screw blades may also lead to increased excavation in granular media, and therefore the effect of number of starts should also be examined further in future work.

4.2   Lessons Learned for System Design and Construction

The construction of ARCSnake V2 revealed the challenges of fully waterproofing the robot. While the cable penetrators, O-rings, and rubber gaskets worked well to create waterproof seals, the shaft seal in the screw block was often not perfect. Therefore, as a solution, we implemented a positive pressure line that held the inside of each segment at positive pressure, so that even if the seal was not perfect, water could not leak into the inner seal tube. Implementing this pressure line turned out to be a fairly easy solution for creating a waterproof prototype, however it requires the robot to be tethered to a positive pressure source. When designing a waterproof screw-propelled snake robot, the method of waterproofing should be very carefully considered.

Another lesson learned is that the motors chosen for such a robot need to be powerful enough for the desired applications, and the torque requirements should consider unexpected resistance in the system. In our robot, the gear mechanism that drives the screw shell had more resistance than expected, which caused the screw shells to be stalled quite easily as motors would hit max torque. This meant we were not able drive the screw shells with the expected force, which limited capability. One of the causes for the extra resistance was that the screw shells were not printed with very high quality. If the screw shell pieces did not fit together properly, this led to grinding with the gears and increased friction. Therefore it is important to consider the extra resistance caused by imperfect manufacturing and make sure the motors chosen can handle this

extra resistance. Machining parts out of metal or using high-precision 3D printers may be critical for obtaining optimal performance.

We demonstrated the swimming capability of ARCSnake V2 by testing it in a real-world environment. Unfortunately, during this field test, there were issues with the motor communication and power transmission. We believe that due to the long length of transmission cables, spikes in current led to a drop in voltage at the load that caused an error flag to raise in the motor's firmware and shut off the motors. Therefore we were forced to limit the current and only power two of the screw motors. This is an important issue that will need to be solved, especially as the plan for future work is to build a robot with six segments instead of three. Therefore another lesson learned is to carefully design the communication and power transmission lines to have low electrical resistance, and ensure it can handle the power requirements of the entire system.

4.3   Future Work

Overall, this work has contributed to the understanding of screw-based locomotion for multi-domain mobility, provided experimental results and performance analysis across different media, and designed a mobile test bed for further characterization of this locomotion mechanism. The construction of ARCSnake V2 has demonstrated the potential of screw-based locomotion in real-world applications and highlighted some of the challenges of designing and constructing a robot for multi-domain mobility. In future work the test bed will be utilized for a more expansive set of experiments. In order to obtain a more complete picture of optimal design choices for screw shells, further experiments should be done for varying lead angle, blade height, and number of starts across all environments. We would also like to further explore the effects of applying an axial load to investigate towing capability, as well as the effect of varying the effective mass of the screw configuration.

ARCSnake V2 is planned to be six segments instead of three, and we have yet to demon-

strate the full snake-like capability of the robot. There are also improvements that can be made to the system design, including decreasing the frictional resistance in the screw drive system and solving the motor communication and voltage lag issues. We plan to solve this issue by increasing the DC voltage for power distribution and adding a DC-DC step-down regulator on each segment to regulate a local voltage for the screw motors. In the future it may be necessary to redesign the system to be self-contained and not rely on a long tether to operate. While there is still much work to be done in this area, and we hope that this thesis will serve as a foundation for further research and development in the field of screw-based locomotion, and proof of concept for a novel exploratory mobile robot.

Appendix A

Modeling Screw Locomotion

A.1 Geometry and Parameters

The screw thread is modeled as the surface of a helicoid bounded an outer radius and the root cylinder, with the thread profile creating two distinct surfaces. The parameterized equation of this helicoid surface in cartesian coordinates is:

$$f(r, \theta) = \langle r\cos\theta, \, r\sin\theta, \, \frac{\ell\theta}{2\pi} \pm (r-R)\tan\phi \rangle, \tag{A.1}$$

where the plus/minus indicates either the leading or trailing thread surface. The corresponding equations for the unit normal vector are:

$$\hat{\mathbf{n}} = \frac{1}{\|\mathbf{n}\|} \langle \frac{\ell}{2\pi}\sin\theta - r\cos\theta\tan\phi, \, -\frac{\ell}{2\pi} - r\sin\theta\tan\phi, r \rangle, \tag{A.2}$$

$$\|\mathbf{n}\| = \sqrt{(\frac{\ell}{2\pi})^2 + r^2(\tan^2\phi + 1)}$$

An alternative formulation can be derived using the angle of the helix, or lead angle, which can be defined as the angle between the x-y plane and the vector tangent to both the thread
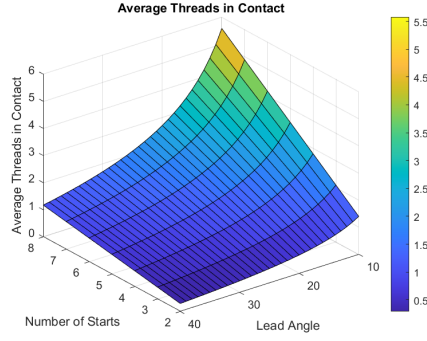
Figure A.1: Average threads in contact. L = 136 mm, r = 72.5mm, ℓ_e = 10mm.

surface and radial vector. This angle will change with *r* according to the relationship

$$\ell = 2\pi r \tan \alpha_r \tag{A.3}$$

which leads to the following formulation of the normal vector:

$$
\begin{aligned}
\mathbf{n}_x &= \frac{1}{\|\mathbf{n}\|}\left(\sin\alpha_r\cos\phi\sin\theta - \cos\alpha_r\sin\phi\cos\theta\right) \\
\mathbf{n}_y &= \frac{1}{\|\mathbf{n}\|}\left(-\cos\alpha_r\sin\phi\sin\theta - \sin\alpha_r\cos\phi\cos\theta\right) \\
\mathbf{n}_z &= \frac{1}{\|\mathbf{n}\|}\cos\alpha_r\cos\phi,
\end{aligned}
\tag{A.4}
$$

$$\|\mathbf{n}\| = \sqrt{\cos^2\phi\sin^2\alpha_r + \cos^2\alpha_r}$$

Using this formulation, if we plug in $\theta = \pi/2$ for example, reveals the same equations used in the standard analysis of static forces for threaded screws.

A.1.1   Threads in contact

One obvious significant factor in the performance of the robot will be how many screw threads can be in contact with the media during the rotation of the screw. Due to the short length of the segments, the number of threads in contact may be very low given certain sets of parameters.

Number of threads in contact, defined as the number of points that intersect a plane tangent to the maximum screw thread radius, produces a square-wave graph as a function of time. It turns out that the average number of threads in contact over one full rotation can be reduced to a simple equation:

$$TIC_{avg} = \frac{Ln_s}{\ell} = \frac{Ln_s}{2\pi r \tan\alpha}. \tag{A.5}$$

In practice, the screw threads are tapered off at the ends of the segment. If the tapered distance, in other words the length along the helix from the start to the point that the thread reaches maximum height, is given by ℓ_e, then the above equation is adjusted as follows:

$$TIC_{avg} = \frac{(L - 2\ell_e)n_s}{\ell} = \frac{(L - 2\ell_e)n_s}{2\pi r \tan\alpha}, \tag{A.6}$$

which is plotted in Fig. A.1 as a function of screw parameters.

A.1.2   Controllable Force Model

For a screw moving on more solid media such as compact sand or gravel, we can take inspiration from vehicle dynamics and terramechanics models to analyze the behavior of our robot. The traction circle is a tool used in vehicle dynamics to visualize the controllable forces generated by the contact between the tire and ground. It describes a region of controllable force that can be generated due to acceleration/braking and steering. The idea is that one can generate a force vector anywhere inside this circle, but once the force vector reaches the limit of the circle the tire will start to slide uncontrollably. The maximum controllable forces in the longitudinal and lateral directions is limited by the frictional properties of the tire/road contact. Specifically, if μ_z and μ_x are the frictional coefficients in the longitudinal and lateral directions, then the maximum force in those directions is given by $N_y\mu_z$ and $N_y\mu_x$, where N_y is the normal force. This leads to the equation [58]
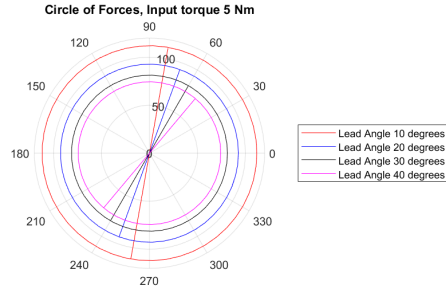
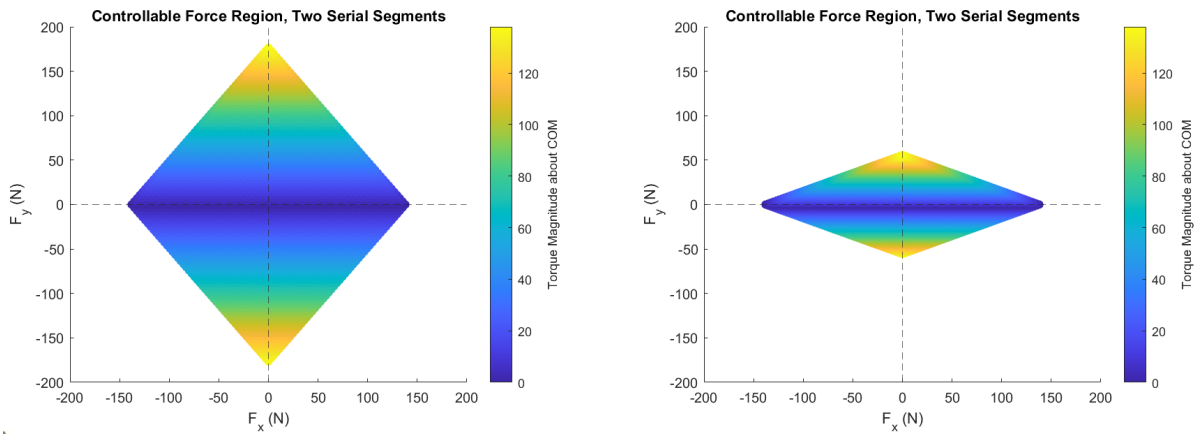**Figure A.2**: Ideal force vectors for various lead angles.

Figure A.3: Controllable Force Region for Two Screw Segments in Series. Left figure is for $\alpha = 10°$, right figure is for $\alpha = 40°$.

$$\frac{F_z^2}{(\mu_z F_N)^2} + \frac{F_x^2}{(\mu_x F_N)^2} \leq 1 \tag{A.7}$$

We can apply a similar concept to visualize the controllable forces of a screw rotor in different scenarios and parameters/configurations. One obvious difference for the case of a single screw, is that we only have one degree of freedom for control, the input torque. In other words, we have no control over steering for a single segment, and thus instead of a circle of forces we simply have single force vectors, as shown in Figure A.2. In this picture, the force output for the given screw parameters can theoretically only move along the lines as the input torque ranges from -5 to 5 Nm (the circles are just shown to visualize the difference in magnitudes).
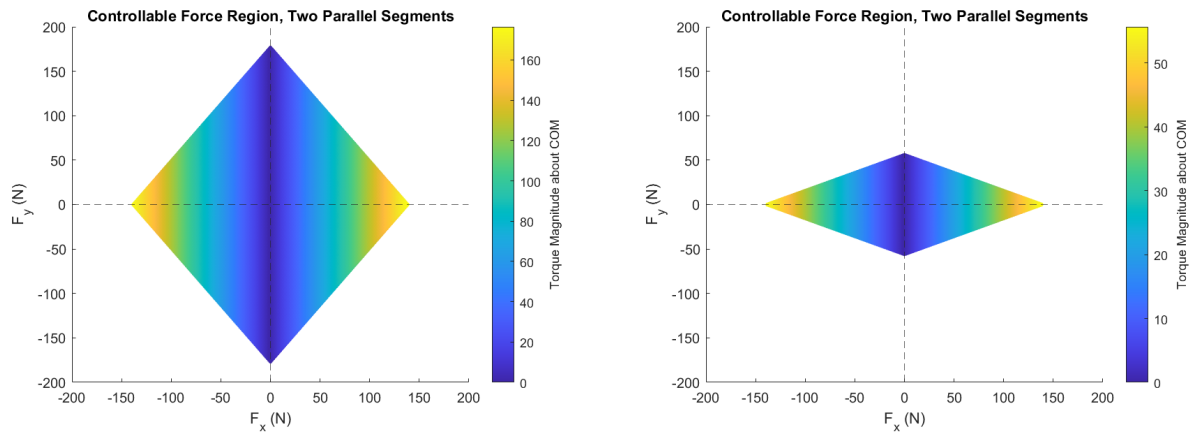
39

Figure A.4: Controllable Force Region for Two Screw Segments in Parallel. Left figure is for $\alpha = 10°$, right figure is for $\alpha = 40°$.

If we consider two screw rotors in parallel (as a rigid body), with opposite-handed screw threads, each of which can independently generate a torque between -5 and 5 Nm, we can consider the region of reachable net force vectors, depicted in Figure A.3. Note that for the majority of possible net force vectors for two segments in series, there will often be a net moment about the center of mass, which is depicted by the color shading in Figure A.3, showing that in this case we can never generate a longitudinal thrust without generating some moment about the center of mass. We can compare this with the controllable force region for two segments in parallel, shown in Figure A.4, where it is evident that the longitudinal thrust can be produced while maintaining zero net torque about the center of mass. If we want to be able to produce thrust without generating a torque about the center of mass for a serial configuration, we need at least three segments.

Bibliography

[1] J. Y. Wong, *Theory of ground vehicles*. John Wiley, 2001.

[2] A. Roennau, G. Heppner, M. Nowicki, J. Zoellner, and R. Dillmann, "Reactive posture behaviors for stable legged locomotion over steep inclines and large obstacles," *2014 IEEE/RSJ International Conference on Intelligent Robots and Systems*, pp. 4888–4894, 2014.

[3] E. Guizzo, "By leaps and bounds: An exclusive look at how boston dynamics is redefining robot agility," *IEEE Spectrum*, vol. 56, no. 12, pp. 34–39, 2019.

[4] W.-S. Chu, K.-T. Lee, S.-H. Song, M.-W. Han, J.-Y. Lee, H.-S. Kim, M.-S. Kim, Y.-J. Park, K.-J. Cho, and S.-H. Ahn, "Review of biomimetic underwater robots using smart actuators," *International Journal of Precision Engineering and Manufacturing*, vol. 13, no. 7, p. 1281–1292, 2012.

[5] R. Li, B. Wu, K. Di, A. Angelova, R. E. Arvidson, I.-C. Lee, M. Maimone, L. H. Matthies, L. Richer, and R. Sullivan, "Characterization of traverse slippage experienced by spirit rover on husband hill at gusev crater," *Journal of Geophysical Research*, vol. 113, no. E12, 2008.

[6] K. Carpenter, A. Thoesen, D. Mick, J. Martia, M. Cable, K. Mitchell, S. Hovsepian, J. Jasper, N. Georgiev, R. Thakker, A. Kourchians, B. Wilcox, M. Yip, and H. Marvi, *Exobiology Extant Life Surveyor (EELS)*, pp. 328–338. ASCE Library, 2021.

[7] F. Richter, P. V. Gavrilov, H. M. Lam, A. Degani, and M. C. Yip, "Arcsnake: Reconfigurable snakelike robot with archimedean screw propulsion for multidomain mobility," *IEEE Transactions on Robotics*, vol. 38, no. 2, pp. 797–809, 2021.

[8] S. Waters and G. A. Aggidis, "Over 2000 years in review: Revival of the archimedes screw from pump to turbine," *Renewable & sustainable energy reviews*, vol. 51, pp. 497–505, 2015.

[9] H. E. Rossell and L. B. Chapman, *Principles of Naval Architecture*. Published by the Society of Naval Architects and Marine Engineers, 1962.

[10] T. Wells, "Improvement in the manner of constructing and of propelling steamboats, denominated the buoyant spiral propeller," U.S. Patent 2400, Dec. 1841.

[11] M. Neumeyer and B. Jones, "The marsh screw amphibian," *Journal of Terramechanics*, vol. 2, no. 4, p. 83–88, 1965.

[12] J. Freeberg, *A study of omnidirectional quad-screw-drive configurations for all-terrain locomotion*. PhD thesis, University of South Florida, Oct. 2010.

[13] D. A. Schreiber, F. Richter, A. Bilan, P. V. Gavrilov, H. M. Lam, C. H. Price, K. C. Carpenter, and M. C. Yip, "Arcsnake: an archimedes' screw-propelled, reconfigurable serpentine robot for complex environments," in *2020 IEEE International Conference on Robotics and Automation (ICRA)*, pp. 7029–7034, IEEE, 2020.

[14] K. Nagaoka, T. Kubota, M. Otsuki, and S. Tanaka, "Development of lunar exploration rover using screw propulsion units," 2009.

[15] J. H. Lugo, M. Zoppi, and R. Molfino, "Design and kinematic modeling of a screw-propelled mobile robot to perform remote explosive scent tracing filter sampling in forest during humanitarian demining," in *Advances in Cooperative Robotics*, pp. 699–715, World Scientific, July 2016.

[16] D. Osiński and K. Szykiedans, "Small Remotely Operated Screw-Propelled Vehicle," in *Progress in Automation, Robotics and Measuring Techniques* (R. Szewczyk, C. Zieliński, and M. Kaliczyńska, eds.), Advances in Intelligent Systems and Computing, (Cham), pp. 191–200, Springer International Publishing, 2015.

[17] W. H. Mayfield, *Development of a Novel Amphibious Locomotion System for Use in Intra-Luminal Surgical Procedures*. PhD thesis, University of Leeds, Aug. 2015.

[18] Y. Kim and D. Kim, "Novel propelling mechanisms based on frictional interaction for endoscope robot," *Tribology Transactions*, vol. 53, no. 2, pp. 203–211, 2010.

[19] H. Liang, Y. Guan, Z. Xiao, C. Hu, and Z. Liu, "A screw propelling capsule robot," in *2011 IEEE International Conference on Information and Automation*, pp. 786–791, June 2011.

[20] T. J. Schwehr, A. J. Sperry, J. D. Rolston, M. D. Alexander, J. J. Abbott, and A. Kuntz, "Toward targeted therapy in the brain by leveraging screw-tip soft magnetically steerable needles," in *HSMR2022 (The 14th Hamlyn Symposium on Medical Robotics)*, 2022.

[21] R. G. Budynas and J. K. Nisbett, *Shigley's mechanical engineering design*, vol. 9. McGraw-Hill New York, 2011.

[22] A. M. Group and B. N. Cole, "Inquiry into amphibious screw traction," *Proceedings of the Institution of Mechanical Engineers*, vol. 175, p. 919–940, June 1961.

[23] H. Dugoff and I. Robert Ehlich, "Model tests of bouyant screw rotor configurations," *Journal of Terramechanics*, vol. 4, no. 3, pp. 9–22, 1967.

[24] D. He and L. C. Long, "Design and analysis of a novel multifunctional screw-propelled vehicle," *2017 IEEE International Conference on Unmanned Systems (ICUS)*, pp. 324–330, 2017.

[25] K. Nagaoka, M. Otsuki, T. Kubota, and S. Tanaka, "Terramechanics-based propulsive characteristics of mobile robot driven by Archimedean screw mechanism on soft soil," in *2010 IEEE/RSJ International Conference on Intelligent Robots and Systems*, pp. 4946–4951, Oct. 2010.

[26] M. Oshima, M. Komoto, and M. Nakamura, "Development of Archimedean Screw Tractor," in *Offshore Technology Conference*, OnePetro, May 1982.

[27] J. K. Hopkins, B. W. Spranklin, and S. K. Gupta, "A survey of snake-inspired robot designs," *Bioinspiration and Biomimetics*, vol. 4, no. 2, pp. 1–10, 2009.

[28] J. Gray, "The mechanism of locomotion in snakes," *Journal of Experimental Biology*, vol. 23, no. 2, pp. 101–120, 1946.

[29] S. Hirose and H. Yamada, "Snake-like robots [tutorial]," *IEEE Robotics & Automation Magazine*, vol. 16, no. 1, pp. 88–98, 2009.

[30] G. Endo, K. Togawa, and S. Hirose, "A self-contained and terrain-adaptive active cord mechanism," *Advanced Robotics*, vol. 13, no. 1, pp. 243–244, 1999.

[31] C. D. Onal and D. Rus, "Autonomous undulatory serpentine locomotion utilizing body dynamics of a fluidic soft robot," *Bioinspiration & biomimetics*, vol. 8, no. 2, p. 26003, 2013.

[32] M. Saito, M. Fukaya, and T. Iwasaki, "Serpentine locomotion with robotic snakes," *IEEE Control Systems Magazine*, vol. 22, no. 1, pp. 64–81, 2002.

[33] T. Kano, T. Sato, R. Kobayashi, and A. Ishiguro, "Decentralized control of scaffold-assisted serpentine locomotion that exploits body softness," *2011 IEEE International Conference on Robotics and Automation*, pp. 5129–5124, 2011.

[34] A. A. Transeth, R. I. Leine, C. Glocker, K. Y. Pettersen, and P. Liljebäck, "Snake robot obstacle-aided locomotion: Modeling, simulations, and experiments," *IEEE Transactions on Robotics*, vol. 24, no. 1, pp. 88–104, 2008.

[35] P. Liljeback, K. Y. Pettersen, Ø. Stavdahl, and J. T. Gravdahl, "Experimental investigation of obstacle-aided locomotion with a snake robot," *IEEE Transactions on Robotics*, vol. 27, no. 4, pp. 792–800, 2011.

[36] Z. Y. Bayraktaroglu, "Snake-like locomotion: Experimentations with a biologically inspired wheel-less snake robot," *Mechanism and Machine Theory*, vol. 44, no. 3, pp. 591–602, 2009.

[37] F. Trebuňa, I. Virgala, M. Pástor, T. Lipták, and L. Miková, "An inspection of pipe by snake robot," *International Journal of Advanced Robotic Systems*, vol. 13, no. 5, pp. 1–12, 2016.

[38] J. Lim, W. Yang, Y. Shen, and J. Yi, "Analysis and validation of serpentine locomotion dynamics of a wheeled snake robot moving on varied sloped environments," in *2020 IEEE/ASME International Conference on Advanced Intelligent Mechatronics (AIM)*, pp. 1069–1074, IEEE, 2020.

[39] C. Wright, A. Buchan, B. Brown, J. Geist, M. Schwerin, D. Rollinson, M. Tesch, and H. Choset, "Design and architecture of the unified modular snake robot," in *IEEE International Conference on Robotics and Automation*, pp. 4347–4354, IEEE, 2012.

[40] S. Ma, Y. Ohmameuda, and K. Inoue, "Dynamic analysis of 3-dimensional snake robots," *2004 IEEE/RSJ International Conference on Intelligent Robots and Systems (IROS)*, pp. 767–772, 2004.

[41] M. Nakajima, M. Tanaka, K. Tanaka, and F. Matsuno, "Motion control of a snake robot moving between two non-parallel planes," *Advanced Robotics*, vol. 32, pp. 1–15, 2018.

[42] Y. Iguchi, M. Nakajima, R. Ariizumi, and M. Tanaka, "Step climbing control of snake robot with prismatic joints," *Sensors*, vol. 22, no. 13, p. 4920, 2022.

[43] H. Marvi, C. Gong, N. Gravish, H. Astley, M. Travers, R. L. Hatton, J. R. Mendelson, H. Choset, D. L. Hu, and D. I. Goldman, "Sidewinding with minimal slip: Snake and robot ascent of sandy slopes," *Science*, vol. 346, no. 6206, pp. 224–229, 2014.

[44] N. Kamamichi, M. Yamakita, K. Asaka, and Z.-W. Luo, "A snake-like swimming robot using ipmc actuator/sensor," in *IEEE International Conference on Robotics and Automation*, pp. 1812–1817, IEEE, 2006.

[45] S. Yu, S. Ma, B. Li, and Y. Wang, "An amphibious snake-like robot: Design and motion experiments on ground and in water," in *2009 International Conference on Information and Automation*, pp. 500–505, 2009.

[46] A. Crespi and A. J. Ijspeert, "Amphibot ii: An amphibious snake robot that crawls and swims using a central pattern generator," in *Proceedings of the 9th international conference on climbing and walking robots*, pp. 19–27, 2006.

[47] A. Crespi and A. J. Ijspeert, "Online optimization of swimming and crawling in an amphibious snake robot," *IEEE Transactions on Robotics*, vol. 24, no. 1, pp. 75–87, 2008.

[48] K. Kouno, H. Yamada, and S. Hirose, "Development of active-joint active-wheel high traversability snake-like robot acm-r4. 2," *Journal of Robotics and Mechatronics*, vol. 25, no. 3, pp. 559–566, 2013.

[49] K. L. Paap, T. Christaller, and F. Kirchner, "A robot snake to inspect broken buildings," in *Proceedings. 2000 IEEE/RSJ International Conference on Intelligent Robots and Systems (IROS 2000)(Cat. No. 00CH37113)*, vol. 3, pp. 2079–2082, IEEE, 2000.

[50] A. Masayuki, T. Takayama, and S. Hirose, "Development of "souryu-iii": connected crawler vehicle for inspection inside narrow and winding spaces," in *2004 IEEE/RSJ International Conference on Intelligent Robots and Systems (IROS) (IEEE Cat. No.04CH37566)*, vol. 1, pp. 52–57, 2004.

[51] M. Arai, Y. Tanaka, S. Hirose, H. Kuwahara, and S. Tsukui, "Development of "souryu-iv" and "souryu-v:" serially connected crawler vehicles for in-rubble searching operations," *Journal of Field Robotics*, vol. 25, no. 1-2, pp. 31–65, 2008.

[52] M. A. Armada, G. Granosik, M. G. Hansen, and J. Borenstein, "The omnitread serpentine robot for industrial inspection and surveillance," *Industrial Robot: An International Journal*, vol. 32, no. 2, pp. 139–148, 2005.

[53] J. Borenstein and A. Borrell, "The omnitread ot-4 serpentine robot," in *2008 IEEE International Conference on Robotics and Automation*, pp. 1766–1767, 2008.

[54] M. Hara, S. Satomura, H. Fukushima, T. Kamegawa, H. Igarashi, and F. Matsuno, "Control of a snake-like robot using the screw drive mechanism," in *Proceedings 2007 IEEE International Conference on Robotics and Automation*, pp. 3883–3888, IEEE, 2007.

[55] J. Gao, X. Gao, W. Zhu, J. Zhu, and B. Wei, "Design and research of a new structure rescue snake robot with all body drive system," in *2008 IEEE International Conference on Mechatronics and Automation*, pp. 119–124, IEEE, 2008.

[56] J. C. McKenna, D. J. Anhalt, F. M. Bronson, H. B. Brown, M. Schwerin, E. Shammas, and H. Choset, "Toroidal skin drive for snake robot locomotion," in *IEEE International Conference on Robotics and Automation*, pp. 1150–1155, IEEE, 2008.

[57] A. Thoesen, S. Ramirez, and H. Marvi, "Screw-powered propulsion in granular media: An experimental and computational study," *2018 IEEE International Conference on Robotics and Automation (ICRA)*, 2018.

[58] R. Brach and M. Brach, "The tire-force ellipse (friction ellipse) and tire characteristics," *SAE Technical Paper Series*, 2011.